Gold Nanorods Seed Coaxial, Cylinder-Phase Domains from Block Copolymer Solutions

Castro S. T. Laicer,[†] Thomas Q. Chastek,[†] Timothy P. Lodge,[†,‡] and T. Andrew Taton*[,†]

Department of Chemistry and Department of Chemical Engineering and Materials Science, University of Minnesota, 207 Pleasant St. SE, Minneapolis, Minnesota 55455

Received July 1, 2005; Revised Manuscript Received September 12, 2005

ABSTRACT: Individual alkanethiol-functionalized gold nanorods act as morphological seeds that specifically template the growth and direction of large, uniform, cylindrical-phase domains from a polystyrene-*block*-polyisoprene (PS-*b*-PI) copolymer solution. Adding less than 0.0001 vol % nanorods switched the preference of domain growth from predominantly spherulitic to almost exclusively single crystalline, with the PI cylinders uniformly aligned in the same direction as each seeding nanorod. Polarized and dark-field optical microscopy on individual domains and small-angle X-ray scattering experiments on bulk material confirmed this specific seeding effect. By contrast, we find that spherical gold nanoparticles and other materials that are commonly used as heterogeneous nucleants in crystallization (e.g., carbon black, talc, and calcium carbonate) failed to promote single-crystalline domain growth in the same material. Mesoscale dynamic modeling of nanorod−copolymer mixtures illustrates these observations in terms of a specific interaction between the surface of the nanorods and the polyisoprene block, which orients the self-assembling polyisoprene cylinders in the nascent domain nucleus.

Introduction

When a diblock copolymer melt is cooled below its characteristic order-to-disorder transition temperature (T_{ODT}), the constituent polymer blocks can spontaneously assemble into nanostructured domains with isotropic (e.g., double-gyroid, body-centered cubic) or anisotropic (e.g., lamellar, hexagonal/cylindrical) morphology, depending on relative block compositions.[1−3] One useful characteristic of morphological anisotropy in the self-assembled material is that it can lead to anisotropic mechanical,[4−6] optical,[7] and electrical[8] properties in the bulk material. As a result, homogeneously aligned block copolymers are particularly attractive candidate materials for applications in which anisotropic solids must be molded or extruded—such as anisotropic elastomers,[9] reflective photonic band gap films,[10,11] and nanoporous membranes.[12−15] Aligned block copolymers are also useful as structural precursors for other nanomaterials.[16−19]

Below T_{ODT}, order in block copolymers originates from spontaneous nucleation and growth of individual, micron-scale domains. Because these domains are not coherently organized, some additional external influence is required to achieve bulk anisotropy in block copolymers. Various methods have been demonstrated to orient these materials in the bulk, including surface confinement,[20−22] templating by surface patterns,[21,23] shear,[24−26] and electric fields.[27−29] In the absence of these external forces, however, bulk order in block copolymers is largely governed by the formation of coherent, ordered domains from the disordered melt. Theoretical and experimental studies of domain nucleation and growth in anisotropic diblock copolymers show that the cylinders or lamellae of the ordered phase can be either homogeneously aligned or radially oriented with respect to the domain nucleus. Sakamato and Hashimoto observed exclusively ellipsoidal grains of uniformly oriented material in transmission electron microscope (TEM) images of lamellar[30,31] and cylindrical[32] copolymer systems. These observations were supported by theoretical studies on spontaneous domain nucleation in diblock copolymers, which showed that oblong domains of uniformly aligned material were preferred over radial growth.[33] However, polarized optical microscopy of phase transitions illustrated that larger ($d > 1\ \mu$m) domains often exhibit spherulitic liquid-crystalline textures.[34,35] In their work on domain growth in concentrated polystyrene-*block*-polyisoprene (PS-*b*-PI) solutions, Chastek and Lodge observed simultaneous growth of both spherulitic and ellipsoidal domain types in optical microscope images of the same samples.[36] The kinetics of nucleation in this system led the authors to conclude that nucleation was heterogeneous, but it was not possible to assign a structural relationship between the nuclei and the domain types. Currently, little experimental work exists on the nature of block copolymer mesophase growth to yield uniformly aligned domains.

This study demonstrates that the growth and orientation of block copolymer grains can be dictated by inorganic nanorods added to a hexagonal block copolymer phase.[36] We hypothesized that block copolymer cylinders would initially be templated by preferential wetting of polyisoprene segments on an alkanethiol-modified gold nanorod surface and that the subsequent growth and orientation of the copolymer domain would be determined by the direction of the nanorod (Scheme 1). Polarized and dark-field optical microscopy and small-angle X-ray scattering experiments on nanorod−copolymer composites were performed to demonstrate this hypothesis. In addition, mesoscale computational modeling suggested a microstructural mechanism for the initial growth of a uniform copolymer domain from each nanorod seed. While a number of reports have

† Department of Chemistry.
‡ Department of Chemical Engineering and Materials Science.
* To whom correspondence should be addressed. E-mail: taton@chem.umn.edu.

10.1021/ma051429j CCC: $30.25
Published on Web 10/19/2005

Scheme 1

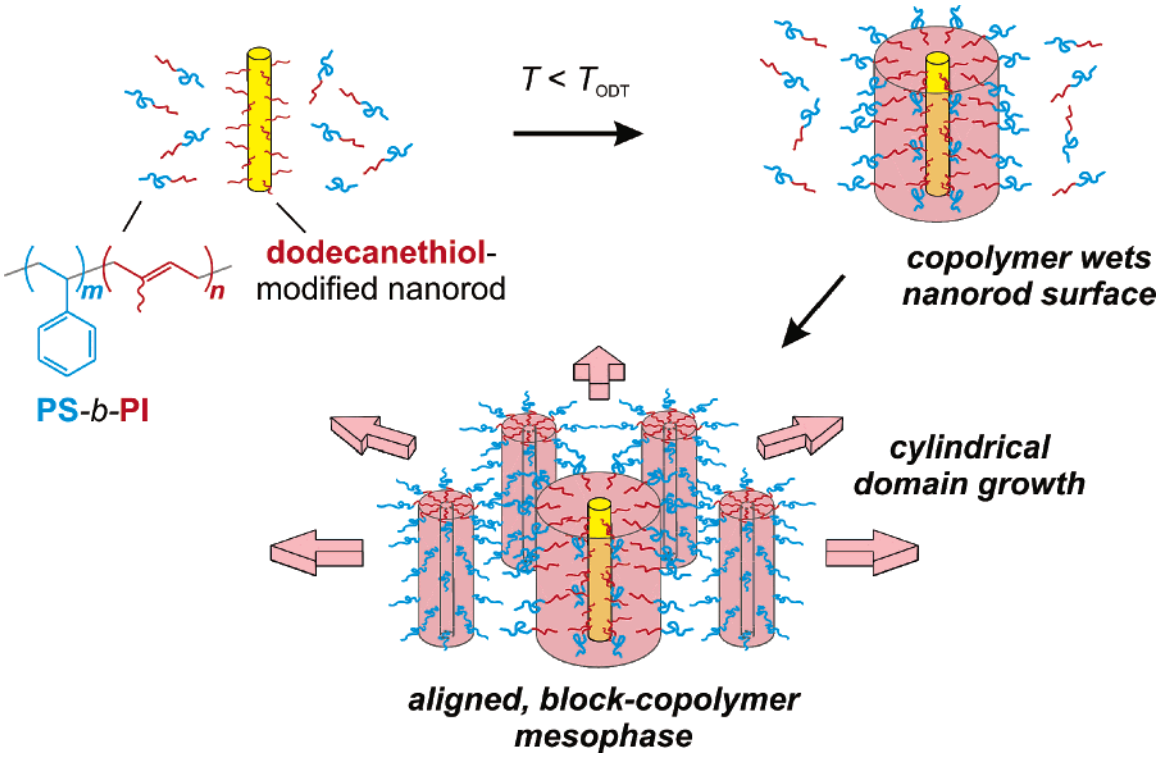

demonstrated that block copolymer mesophases can be used to organize suspended nanoparticles,[37−40] to our knowledge this is the first demonstration that the converse is also true—that suspended nanostructures can be used to direct nanoscale block copolymer assembly.

Experimental Section

Materials. Two model poly(styrene-*b*-isoprene) diblock copolymers with slightly different block lengths were investigated. The block copolymers are denoted "SI(A-B)" based on M_n (kg/mol) of the constituent polystyrene (A) and polyisoprene (B) blocks. SI(15-13) ($M_n = 2.76 \times 10^4$ g/mol; $M_w/M_n = 1.04$) was synthesized as previously described.[41] SI(18-12) ($M_n = 2.98 \times 10^4$ g/mol; $M_w/M_n = 1.02$) was purchased from Polymer Source Inc. (Dorval (Montreal), Canada; product no. P143-SIp). Polymer solutions were prepared gravimetrically by dissolving SI(15-13) and SI(18-12) samples in dibutyl phthalate (DBP, Aldrich) and CH_2Cl_2 cosolvent with stirring. CH_2Cl_2 was subsequently removed under mild nitrogen purge to yield final polymer compositions of 48.5 wt % SI(15-13) and 47 wt % SI(18-12) in DBP.

Gold Nanorod Synthesis. Gold nanowires were prepared by electroless reduction of $Na_3Au(SO_3)_2$ gold plating solution (Oromerse SO B, Technic Inc.) in track-etched polycarbonate membranes (Whatman) with 80 nm pore diameter and 6 μm pore length, following published procedures.[42] Nanowires were isolated by dissolving the membrane in CH_2Cl_2, followed by brief (5 s) sonication to release the wires from undissolved polymer. The resulting bluish brown suspension of gold nanowires was decanted from macroscopic gold film particulates. The gold nanowire suspension was further diluted with CH_2Cl_2 to a total volume of 60 mL. The concentration of this suspension was determined to be 2.43×10^7 Au rods/mL (2.87×10^{-4} M) by ICP-MS analysis.[43] An extinction coefficient of $\epsilon_{580} = 8.21 \times 10^2$ M^{-1} cm^{-1} was measured from UV−vis spectroscopy of the nanorod solution, and this value was used to determine nanorod concentrations in all future experiments.

Surface Modification of Gold Nanowires. Nanowires were modified by addition of 1-dodecanethiol (70 μL) to a 20 mL aliquot of a 2.87×10^{-4} M stock gold nanowire suspension. The solution was mixed on a mechanical shaker for 20 h at room temperature. The nanowires were allowed to settle, and the supernatant was decanted. The remaining nanowire suspension was diluted with CH_2Cl_2, and the washing procedure was repeated three times before final redispersion of gold nanowires in 20 mL of CH_2Cl_2. The concentration of this suspension was determined to be 2.43×10^7 Au rods/mL (2.82×10^{-4} M) by optical absorbance.

Composite Materials. Composite materials were prepared by titrating CH_2Cl_2 suspensions of 1-dodecanethiol-modified gold nanowires (1.20×10^7 Au rods/mL, 1.41×10^{-4} M) into preweighed amounts of SI(15-13)−DBP and SI(18-12)−DBP mixtures. Solvent was then removed while stirring samples under a nitrogen purge until a gravimetric end point was reached to give composite samples with concentrations of 2.22×10^6 Au rods/g of SI−DBP. Control composite samples of SI(18-12)−DBP with spherical gold nanoparticles, spherical carbon black, talc, and calcium carbonate nucleants were prepared similarly.[43]

Scanning Electron Microscopy (SEM). SEM images were obtained with a Hitachi S-800 field-emission gun scanning electron microscope at an accelerating voltage of 5.0 kV.

Polarized Optical Microscopy (POM). POM was performed with a Nikon Optiphot polarized-light microscope, fitted with a Brace-Koehler type (1/20 λ) compensator. Samples were prepared by pressing 150 μm thick films of composite and pure polymer solutions either between two glass slides or between a gridded glass coverslip (Electron Microscopy Sciences, Hatfield, PA) and a plain glass coverslip. Single-sided adhesive tape was used as a spacer to dictate sample thickness. The photoetched glass coverslip was placed such that the plain face was in physical contact with the sample. Sample temperature was controlled by a Linkam Scientific Instruments heat stage to an accuracy of ±0.10 °C. Transition temperatures for SI(18-12)−DBP pure material ($T_{ODT} = 46.1$ °C) and SI(18-12)−DBP−Au composite ($T_{ODT} = 45.8$ °C) were determined by the initial disappearance of birefringence in samples that had been first annealed at 40 °C ($T < T_{ODT}$) for 5 min prior to heating at a rate of 0.30 °C/min. Transition temperatures for SI(18-12)−DBP composited with carbon black ($T_{ODT} = 46.2$ °C), spherical gold nanoparticle ($T_{ODT} = 46.3$ °C), talc ($T_{ODT} = 46.3$ °C), and $CaCO_3$ ($T_{ODT} = 45.8$ °C) were measured similarly.

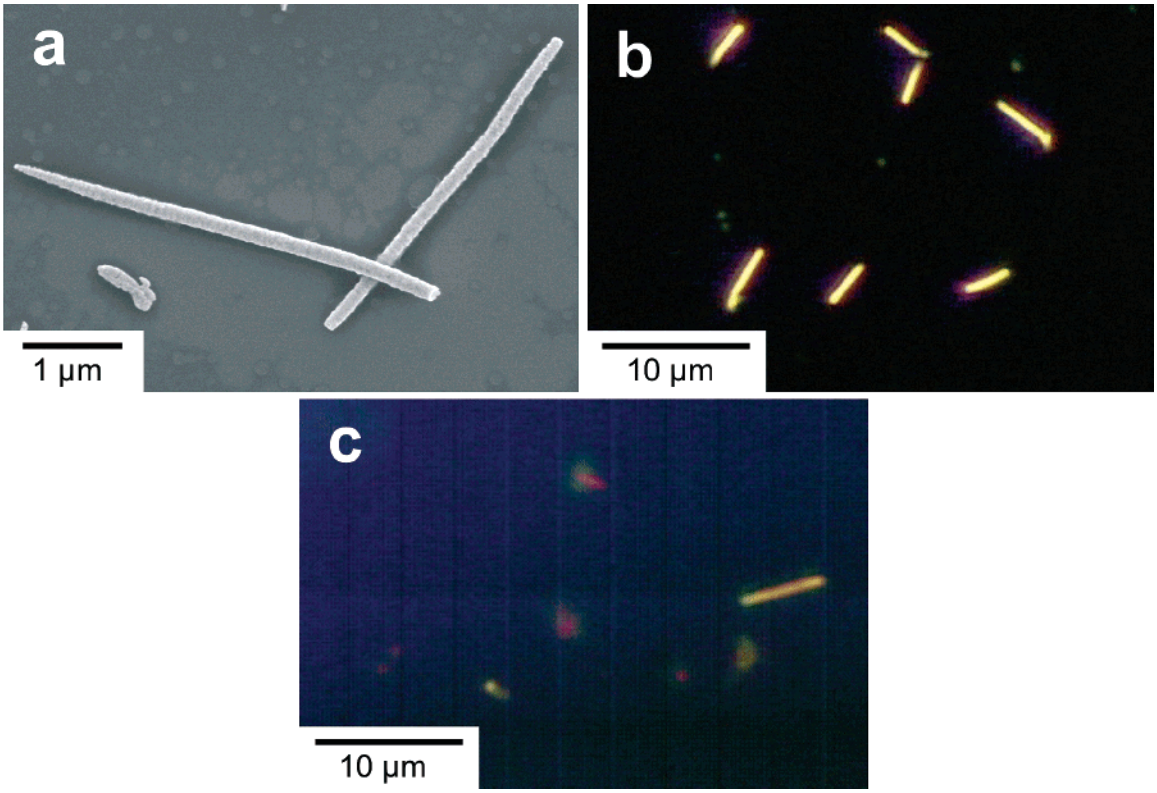

Figure 1. (a) Typical SEM image of gold nanowires (180 nm diameter, 3−6 μm length) drop-coated on a silicon wafer substrate and allowed to dry. The diameters of the nanowires were consistently larger than the reported nominal pore diameter of the polycarbonate membrane templates, consistent with previously published syntheses.[50] Though most of the material synthesized was nanorods, smaller pieces of debris were also observed (<1% of observed objects). (b) Dark-field optical image of the same gold nanowires drop-coated on a glass substrate and allowed to dry. (c) Dark-field optical image of Au nanorods dispersed in SI−DBP.

Static birefringence measurements of T_{ODT} values for the pure SI(18-12)−DBP and Au−SI(18-12)−DBP composite samples were comparable to POM measurements.[43] For POM analysis of domain growth, samples were first annealed at 45 and 55 °C ($T > T_{ODT}$) for SI(15-13) and SI(18-12) materials, respectively. Samples were annealed in the disordered state for at least 5 min prior to a rapid temperature quench to $T < T_{ODT}$. Time-resolved images were collected after samples were quenched and held at constant temperature.

Optical Microscopy: Reflected Dark Field. Optical images of gold nanowires were obtained with a Nikon Optiphot-Pol optical microscope operated in reflected dark-field illumination mode. Incident illumination and detection of scattered light from gold nanowires was performed with a 50× bright-/dark-field objective lens. In the case of gold nanowires embedded in polymer matrices, materials previously imaged by POM were used directly. These samples were frozen in liquid nitrogen so that the top (nonphotoetched) glass cover slide could be removed before imaging; we found this step was necessary to eliminate focal aberration. Then, the point of nucleation for a given block copolymer grain was relocated using bright-field optics and the photoetched markings as positional guides. Any nanorods at this location were then imaged with dark-field optics.

Small-Angle X-ray Scattering (SAXS). SAXS measurements were conducted on a 2-D 2m SAXS instrument at the University of Minnesota Materials Characterization Facility. The instrument consists of a Rigaku RU-200BVH rotating anode X-ray generator to produce a Cu Kα X-ray beam with a wavelength of 1.54 Å. SAXS patterns were measured by focusing the X-ray beam with Franks mirrors onto a 2-D area detector (Siemens HI-STAR) positioned ∼2 m behind the sample. Samples were placed on a heating block with liquid cooling capabilities and a temperature range of 0−200 °C. The sample chamber was exposed to a continuous flow of helium, while the alignment optics and flight tube were under vacuum. Samples were prepared by sealing polymer−nanorod mixtures in 2 mm quartz capillaries (Charles Supper Co.). Capillaries were sealed with a high-temperature silicone glue. Temperature programs began by annealing samples in the disordered state at 55 °C for 5 min prior to a rapid quench to 49.5 °C. Samples were then sequentially cooled in 0.5 °C increments, and annealed for 30 min at each temperature, to determine the T_{ODT} (47.5 °C). Samples were finally annealed 0.5 °C below T_{ODT} for 70 min prior to measurement. Exposure times were 10 min at each temperature.

Mesoscale Modeling. Simulations were performed using the MESODYN module of Materials Studio (Accelrys, San Diego, CA). Parameters for the simulation are given in the Supporting Information.

Results and Discussion

PS-*b*-PI Block Copolymers. To investigate templating and growth of cylindrical-phase domains by gold nanorod nucleants, we chose to composite nanorods with PS-*b*-PI plasticized with DBP (SI-DBP). The phthalate plasticizer preferentially swells the PS block and allows for large, well-defined grains to form due to increased polymer chain mobility. The relationship between phase morphology and polymer composition in SI−DBP mixtures has been previously characterized by Lodge et al.[41] For this study we selected polymer−DBP fractions that are known to form cylindrical morphologies in which polyisoprene cylinders are surrounded by a polystyrene−plasticizer matrix. Chastek and Lodge previously showed that cooling SI(15-13)−DBP below T_{ODT} yielded both spherulitic and ellipsoid-shaped domains,[36] and we investigated this same material in this study. We also investigated an SI(18-12)−DBP mixture that exhibited cylindrical morphology with *d*-spacing of 22 nm (verified by SAXS[43]) and showed the same pattern of domain growth as SI(15-13)−DBP. Overall, we found that these

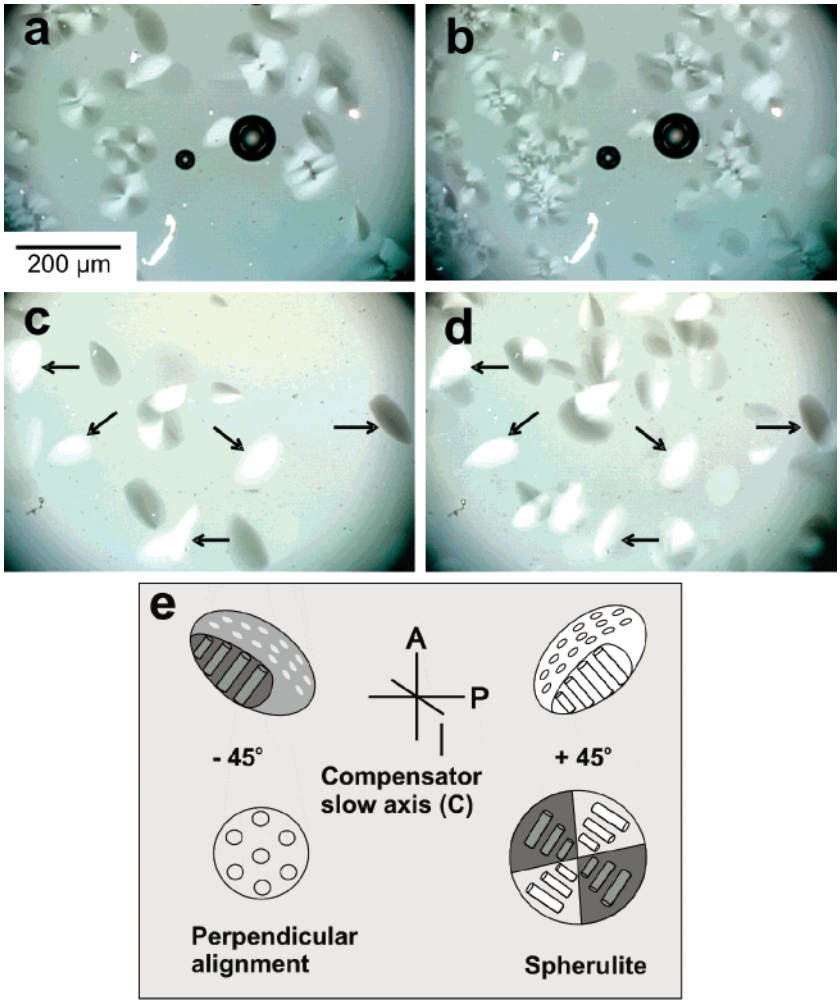

Figure 2. POM images of grains nucleated at identical locations during repeated temperature quenches. Pure SI(18-12) sample after quenching from $T > T_{ODT}$ to (a) 45.7 °C and (b) 45.5 °C. Au−SI(18-12) composite sample after quenching from $T > T_{ODT}$ to (c) 45.3 °C and (d) 45.0 °C. Samples were annealed at 55.0 °C for 5 min prior to quenching below T_{ODT}. Black arrows in POM micrographs (c) and (d) point out the relative positions of ellipsoidal grains nucleated in the same location in the two quenches. (e) Schematic representation of the relative orientations of nucleated grains, polarizer (P), analyzer (A), and compensator (C) and corresponding shading patterns.[36] Block copolymer cylinders are oriented along the short axis of the ellipsoidal domains and along a diameter of spherulites. The dark circles in (a) and (b) are trapped air bubbles used as reference markers.

copolymer−plasticizer mixtures yielded large domains that were straightforward to image and characterize relative to those formed from pure SI material.

Gold Nanorod Nucleants. Au nanorods were used as model nucleants because (1) they can be synthesized in controllable lengths and diameters, (2) the interaction between the nanorod surface and a copolymer block can be modulated by functionalizing the surface with thiol ligands, and (3) polymer-embedded nanorods can be located and imaged by dark-field optical microscopy. In this study, the surfaces of 180 nm diameter, 3−6 μm long Au nanorods were modified with 1-dodecanethiol. We assumed that the polyisoprene block of PS-*b*-PI would selectively interact with the alkane-functionalized surfaces of the nanorods, based on previous studies of selective assembly of PS-*b*-PI[44] and PS/PI blends[45,46] at hydrocarbon and polyolefin interfaces. To minimize mechanical stress and breakage of the nanorods,[47] we blended the rods with SI-DBP by codissolving the components in volatile solvent and then evaporating the solvent away. The physical properties of the polymer and nanorods did not appear to be affected by this procedure. SEM images of Au nanorods recovered by dissolving away the polymer host looked identical to those of the starting rods. Similarly, SAXS measurements of SI(18-12)−DBP showed the same morphology and *d* spacing for samples with and without Au nanorod additives.[43]

Because of their extremely large scattering cross sections, individual gold nanorods could also be located and imaged by dark-field optical microscopy.[48,49] Nanorods deposited onto flat substrates appeared bright yellow-orange under oblique illumination (Figure 1b). Polymer-dispersed nanowires could also be imaged through the polymer host by this technique, at shallow depths (Figure 1c). Polymer-embedded nanorods appeared dimmer and appeared particularly faint when they were too deeply embedded or pointed too closely parallel to the viewing angle. Nonetheless, the orientation of many of the nanorods in the polymer could be successfully determined by dark-field imaging.

Analysis of Au Nanorod−PS-*b*-PI Composite Samples by Polarized Optical Microscopy (POM). To investigate how embedded nanorods affected the evolution of order in PS-*b*-PI, domain seeding and growth were initiated by cooling samples below T_{ODT} and were imaged by time- and temperature-resolved POM. In the absence of nanorods, domain growth in SI(18-12)−DBP was consistent with previous observations[36] in which both spherulites and ellipsoidal do-

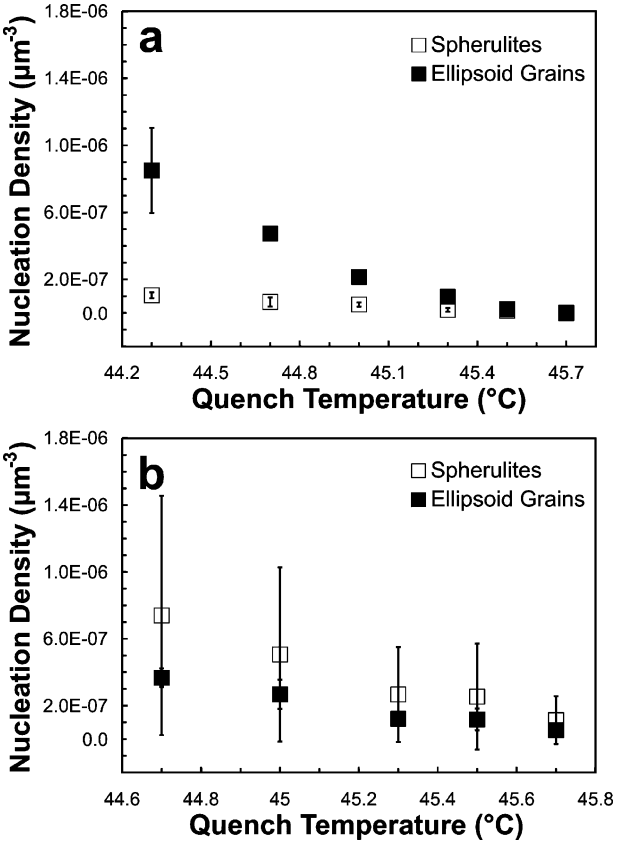

Figure 3. Nucleation density of ellipsoid and spherulite grains at varying quench temperatures for (a) Au−SI(18-12)−DBP and (b) SI(18-12)−DBP. Samples were annealed in the disordered state at 55 °C prior to quenching to each final temperature, and then domains were identified and counted from polarized microscope images. Over 1500 domains were counted from four separately prepared samples to obtain the data shown above. The large deviation ranges for values in (b) are due to variation within each sample rather than sample-to-sample variation or measurement error.

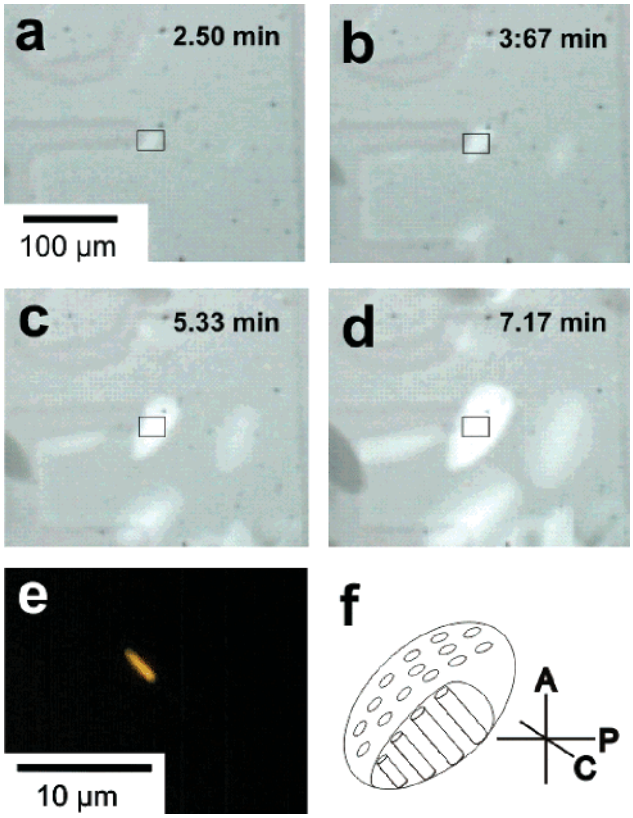

Figure 4. (a−d) Time-lapsed POM images of nucleation and growth of an ellipsoid domain for an Au−SI(15-13)−DBP composite sample quenched from $T > T_{ODT}$ to 37.0 °C. The sample was annealed in the disordered state at 45 °C prior to quenching below the T_{ODT}. The box is provided to highlight the nucleation position of the ellipsoidal grain of interest and marks the same area as is shown in (e). (e) Dark-field image of a gold nanorod nucleant particle and (f) schematic showing orientation of cylinders within the nucleated ellipsoid domain. The photoetched coverslip markings in the POM micrographs were used as positional reference markers.

mains were observed (Figure 2a). During repeated melting and cooling cycles, the same types of domains grew from the same locations, indicating heterogeneous nucleation (Figure 2b). Multiple rounds of filtration did not change this behavior, and the identity and size of the nucleants in these SI(18-12)−DBP samples is not known.

POM measurements of SI−DBP−Au nanorod composite samples, on the other hand, produced predominantly uniformly aligned, ellipsoidal domains when cooled below T_{ODT} (Figure 2c). Again, nucleation occurred in the same locations when samples were exposed to repeated melting and cooling cycles (Figure 2d). The number of nucleated grains correlated with the degree of undercooling,[51] but the prevalence of uniformly aligned ellipsoidal domains did not vary (Figure 3). When domain types were counted in multiple samples, the pure material showed predominantly spherulitic and ellipsoidal domains (Figure 3b), while the composite sample showed almost exclusively ellipsoids (Figure 3a). Although the efficiency of domain nucleation by nanorods was not quantified, it is not 100%. For example, we estimate that the volume of polymer shown in Figure 2c should contain ∼140 Au nanorods (based on overall concentration), substantially more than the number of observed domains.

Cylinder Templating and Growth by Gold Nanorods. To correlate individual domains with nanorod nucleants, embedded rods were located and imaged directly using dark-field microscopy. Figure 4 shows time-lapsed POM images of an Au−SI(15-13)−DBP composite sample as an ellipsoidal domain grows below T_{ODT}. After cooling further to room temperature, the same region of the sample was scanned under dark-field illumination, using the underlying photoetched markings on the coverslip as a guide. One nanorod was located at the center of the domain (Figure 4e), oriented roughly perpendicular (78 ± 5°) to the long axis of the domain. Because the cylinders of block copolymer are also oriented perpendicular to the long axis, they are coaxially oriented with respect to the nanorod. Further imaging of domains and nanorods showed other domains in which copolymer cylinders were aligned parallel to Au nanorod nucleants (Figure 5). Nanorods were not imaged at the center of every domain, probably because Au nanorods that were embedded deep within the polymer matrix were not visible. In nearly all cases (>90%) where a gold nanorod was associated with a domain, and its orientation could be determined, it was pointed within 15° of the short axis of the ellipsoidal copolymer domain (Figure 5, S1[43]). Other types of dispersed nucleants—including spherical gold nanoparticles (d = 108 nm), carbon black (d = 11 nm), talc (d = 2 μm), and $CaCO_3$ (d = 1.3−1.8 μm)—failed to selectively promote nucleation of homogeneous domains in the SI(18-12)−DBP melt and instead yielded roughly equal

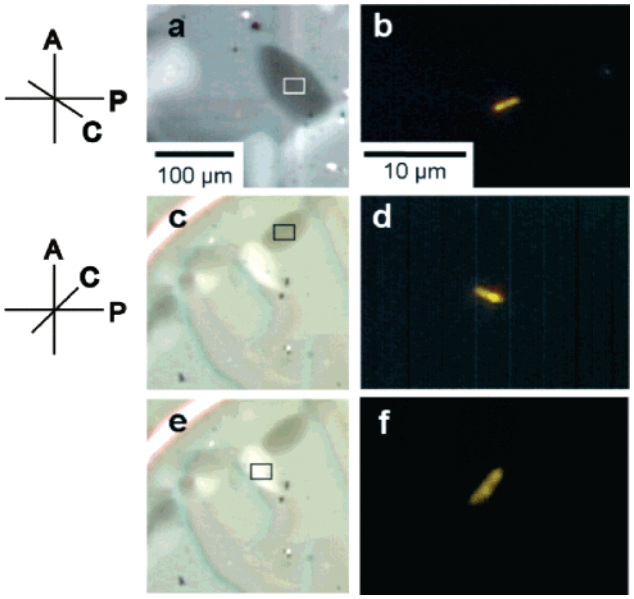

Figure 5. POM images of ellipsoid domains and corresponding dark-field optical microscopy images of gold nanorods imaged within the composite polymer matrix. Images of gold nanorods were obtained at identical positions to locations of nucleated domains in the POM images. Part (b) was obtained for the grain indicated in (a). Images (d) and (f) were obtained for grains in (c), and (e), respectively, as indicated by the boxes provided in the POM micrographs. Image (a) is a POM image of an Au−SI(15-13) composite sample, and image (c) is a POM image of an Au−SI(18-12) composite sample. The relative orientation of polarizers (P, A) and compensator (C) are shown to the left of the POM micrographs.

numbers of spherulites and ellipsoids.[43] Although it was not possible to image these nucleants in situ, we conclude from these experiments that Au nanorods have a unique nucleating influence on cylinder-phase SI−DBP.

SAXS Analysis of Nucleated Domains. As observed in Figure 2, cooled samples of Au−SI−DBP consists almost exclusively of ellipsoidal domains. To confirm that these were single-crystalline, cylinder-phase domains, we performed temperature-resolved SAXS measurements on SI−DBP in both the presence and absence of nanorods. Chastek and Lodge previously reported that an individual, single-crystalline domain could be located in pure SI(15-13)−DBP by scanning a slowly annealed sample with the SAXS beam.[36] By contrast, in the presence of Au nanorods, 2-D SAXS patterns (Figure 6a) and azimuthal integration spectra (Figure 6b) from SI(18-12)−DBP showed several distinct pairs of peaks separated by 180° when the beam was trained on virtually any region of the sample. Each pair of peaks represents one of multiple large, single-crystalline domains within the 4 mm^2 X-ray beam area whose orientation is not coincident with the beam. T_{ODT} determined from the appearance of peaks in SAXS (47.5 °C) was comparable to values determined from polarized microcoscopy measurements (Figure S7).[43] Overall, these observations support the hypothesis that Au nanorods preferentially induce the nucleation and growth of homogeneous cylinder-phase domains in DBP-plasticized PS-*b*-PI.

Mesoscale Modeling. To better understand the physical mechanism behind nanorod seeding, we simulated the response of a block copolymer melt to a single, embedded nanorod using dynamic density functional theory (DDFT).[52−58] In polymer DDFT, polymer segments are modeled as Gaussian strings of beads, and the distribution of bead density is solved by the appropriate Langevin equation of motion.[53,54,57] PS-*b*-PI was simulated as chains with composition A_3B_7 (A = PI, B = PS), for which self-consistent mean-field (SCMF) theory predicts a cylindrical phase ($f_A = 0.30$, $\chi N \approx 19$).[59] Chains were confined to a rectangular volume with a cylindrical void in the center that represented a static nanorod. Energetic interaction parameters between A beads and the surface of the void were defined as negative in order to model favorable interactions between PI segments and an alkanethiol-modified Au nanorod. The organization of the chains in the box was then allowed to evolve over time to simulate cooling below T_{ODT}. During the early stages of the simulation (τ = 200 steps), phase segregation was selectively initiated by the formation of a wetting layer of A beads on the nanorod surface while the melt in the bulk material was still homogeneously mixed (Figure 7b). This surface layer templated successive lamellae of diblock chains around the rod. Only after further simulation time were these lamellae converted to copolymer cylinders oriented in the same direction as the nanorod (Figure 7c−e), followed by propagation of

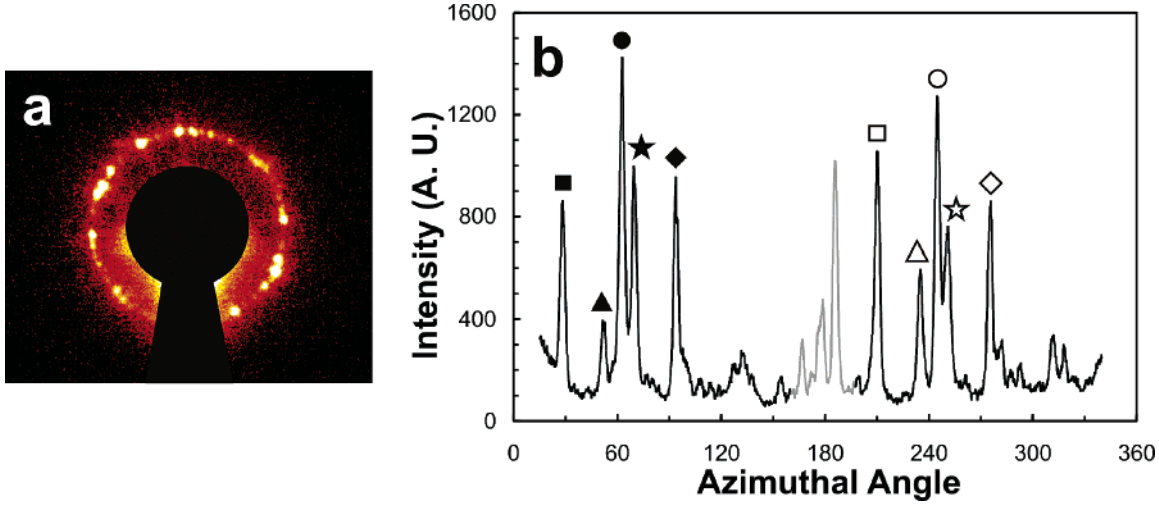

Figure 6. (a) 2-D SAXS patterns and (b) corresponding azimuthal integration of the principle Bragg reflection for a Au−SI(18-12) composite sample. The large black mask in (a) is provided to block strong parasitic scattering from the instrument and sample. Possible partners for the shaded peaks at ~180° would be blocked by the mask. SAXS measurement was made at 46.5 °C.

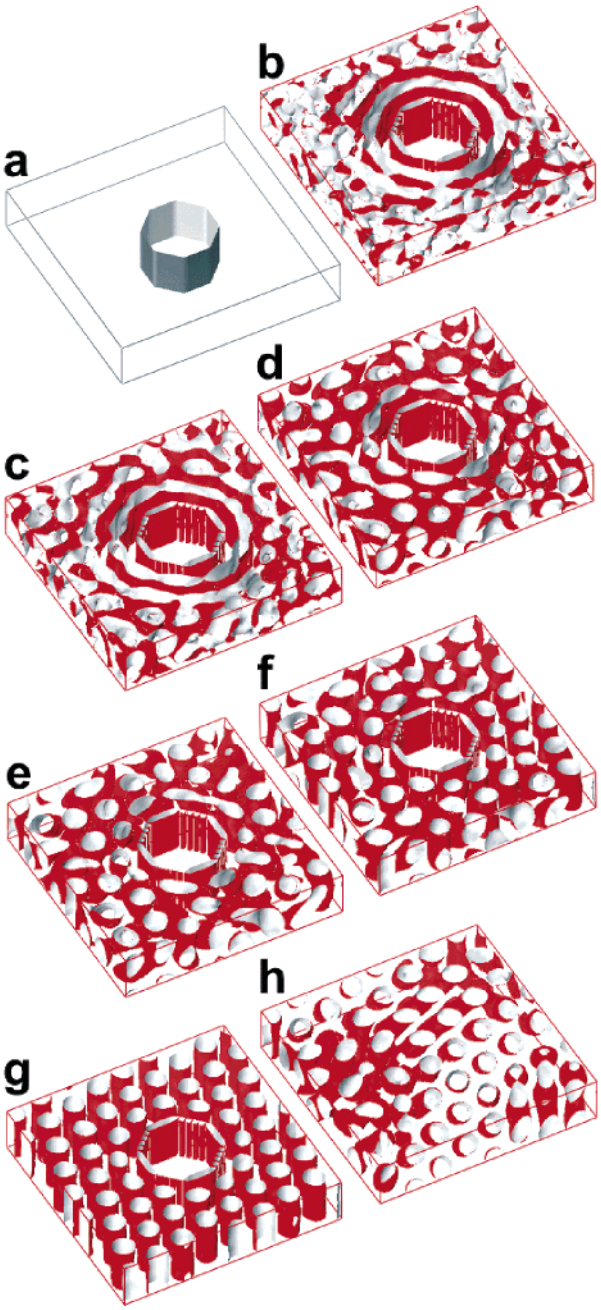

Figure 7. Isodensity surfaces of A beads for an A_3B_7 melt in a cubic grid box at various dimensionless time steps, τ. (a) View of nanorod particle in a grid box, (b) morphology of A beads with nanorod additive at $\tau = 200$, (c) $\tau = 400$, (d) $\tau = 600$, (e) $\tau = 2000$, (f) $\tau = 8000$, and (g) $\tau = 16\,000$. (h) Isodensity surfaces of A beads for a bulk A_3B_7 melt without a nanorod nucleant at $\tau = 16\,000$.

cylinder alignment into the surrounding material (Figure 7f,g). Defects in cylinder orientation were gradually eliminated to produce homogeneously aligned, hexagonally packed cylinder nanostructures, in which the net orientation of cylinders is determined by the nanorod particle. For comparison, identical simulations performed on an A_3B_7 copolymer in the same simulation volume but without the cylindrical void yielded a phase in which the cylinders were less coherently organized and for which long-range ordering occurred much more slowly (Figure 7h, S3[43]). Coaxial ordering also failed to develop when the energetic interaction between the nanorod and block A was insufficiently negative or when the ratio of templating rod diameter to copolymer phase periodicity was too small (<0.5) or too large (>5). Our observation that mesophase order propagates from the surface of a nanorod[60,61] is analogous to previous theoretical[54,62,63] and experimental[64−68] work on alignment of cylindrical copolymer domains parallel to flat surfaces. As in our studies, these reports illustrate that domain organization near flat surfaces is generally initiated by selective surface wetting by one of the copolymer blocks, followed by propagation of order into the polymer bulk. For simplicity, our simulations focused only on the organization of material in the immediate vicinity of the nanorod, and it is not clear how time or length scale or energetics in the DDFT model translate to experimental results. Nevertheless, we propose that these simulations illustrate how selective morphological seeding could be responsible for micron-scale order in the surrounding, ellipsoidal domains of Au−SI−DBP composite.

Conclusions

This work has demonstrated the selective nucleation of cylindrical-phase SI block copolymer domains by Au nanorod nucleants. Moreover, we have also shown that the orientation of the copolymer domains is dictated by that of the nanorods. Because very little nanorod material is required to induce organization in a large volume of copolymer, we propose that nanorod templating could be used as a way of controlling mesophase organization throughout block copolymer materials without influencing the copolymers' inherent physical properties. We are currently investigating methods toward bulk nanocomposite material alignment by orientation of matrix embedded nanorod nucleants with externally applied fields. Alternatively, nanofabricated arrays of vertical aligned nanowires[69,70] could also be potentially used to achieve the same goal. We anticipate that if this method is broadly applicable to other materials, it might contribute toward the development of bulk aligned block copolymer/inorganic nanocomposites with technologically relevant anisotropic mechanical, electrical, and optical properties.

Acknowledgment. We thank the Research Corporation (Research Innovation Award RI0964), the Alfred P. Sloan Foundation (Fellowship BR-4527 to T.A.T.), the National Science Foundation (DMR-0406656), and the University of Minnesota for financial support of this research. The computational modeling was supported in part by the University of Minnesota Supercomputing Institute.

Supporting Information Available: Additional polarized and dark-field microscope images, control composites, details of mesoscale modeling, and materials characterization. This material is available free of charge via the Internet at http://pubs.acs.org.

References and Notes

(1) Hamley, I. W. *The Physics of Block Copolymers*; Oxford University Press: Oxford, 1998.
(2) Lodge, T. P. *Macromol. Chem. Phys.* **2003**, *204*, 265−273.
(3) Bates, F. S.; Fredrickson, G. H. *Annu. Rev. Phys. Chem.* **1990**, *41*, 525−57.
(4) Arridge, R. G. C.; Folkes, M. J. *J. Phys. D: Appl. Phys.* **1972**, *5*, 344−58.
(5) Honeker, C. C.; Thomas, E. L. *Chem. Mater.* **1996**, *8*, 1702−1714.
(6) Hahn, H.; Lee, J. H.; Balsara, N. P.; Garetz, B. A.; Watanabe, H. *Macromolecules* **2001**, *34*, 8701−8709.

(7) Abuzaina, F. M.; Garetz, B. A.; Mody, J. U.; Newstein, M. C.; Balsara, N. P. *Macromolecules* **2004**, *37*, 4185−4195.
(8) Amundson, K.; Helfand, E.; Davis, D. D.; Quan, X.; Patel, S. S.; Smith, S. D. *Macromolecules* **1991**, *24*, 6546−8.
(9) Folkes, M. J.; Keller, A. *Polymer* **1971**, *12*, 222−36.
(10) Valkama, S.; Kosonen, H.; Ruokolainen, J.; Haatainen, T.; Torkkeli, M.; Serimaa, R.; ten Brinke, G.; Ikkala, O. *Nat. Mater.* **2004**, *3*, 872−876.
(11) Edrington, A. C.; Urbas, A. M.; DeRege, P.; Chen, C. X.; Swager, T. M.; Hadjichristidis, N.; Xenidou, M.; Fetters, L. J.; Joannopoulos, J. D.; Fink, Y.; Thomas, E. L. *Adv. Mater.* **2001**, *13*, 421−425.
(12) Hashimoto, T.; Tsutsumi, K.; Funaki, Y. *Langmuir* **1997**, *13*, 6869−6872.
(13) Liu, G.; Ding, J.; Stewart, S. *Angew. Chem., Int. Ed.* **1999**, *38*, 835−838.
(14) Xu, T.; Stevens, J.; Villa, J.; Goldbach, J. T.; Guarini, K. W.; Black, C. T.; Hawker, C. J.; Russell, T. P. *Adv. Funct. Mater.* **2003**, *13*, 698−702.
(15) Zalusky, A. S.; Olayo-Valles, R.; Wolf, J. H.; Hillmyer, M. A. *J. Am. Chem. Soc.* **2002**, *124*, 12761−12773.
(16) Thurn-Albrecht, T.; Schotter, J.; Kastle, G. A.; Emley, N.; Shibauchi, T.; Krusin-Elbaum, L.; Guarini, K.; Black, C. T.; Tuominen, M. T.; Russell, T. P. *Science* **2000**, *290*, 2126−2129.
(17) Templin, M.; Franck, A.; Du Chesne, A.; Leist, H.; Zhang, Y.; Ulrich, R.; Schadler, V.; Wiesner, U. *Science* **1997**, *278*, 1795−1798.
(18) Lopes, W. A.; Jaeger, H. M. *Nature (London)* **2001**, *414*, 735−8.
(19) Ha, J.-M.; Wolf, J. H.; Hillmyer, M. A.; Ward, M. D. *J. Am. Chem. Soc.* **2004**, *126*, 3382−3383.
(20) Harrison, C.; Adamson, D. H.; Cheng, Z.; Sebastian, J. M.; Sethuraman, S.; Huse, D. A.; Register, R. A.; Chaikin, P. M. *Science* **2000**, *290*, 1558−1561.
(21) Rockford, L.; Mochrie, S. G. J.; Russell, T. P. *Macromolecules* **2001**, *34*, 1487−1492.
(22) Cheng, J. Y.; Mayes, A. M.; Ross, C. A. *Nat. Mater.* **2004**, *3*, 823−828.
(23) Kim, S. O.; Solak, H. H.; Stoykovich, M. P.; Ferrier, N. J.; de Pablo, J. J.; Nealey, P. F. *Nature (London)* **2003**, *424*, 411−414.
(24) Hamley, I. W. *Curr. Opin. Colloid Interface Sci.* **2000**, *5*, 342−350.
(25) Morrison, F. A.; Winter, H. H.; Gronski, W.; Barnes, J. D. *Macromolecules* **1990**, *23*, 4200−5.
(26) Chen, Z.-R.; Kornfield, J. A.; Smith, S. D.; Grothaus, J. T.; Satkowski, M. M. *Science* **1997**, *277*, 1248−1253.
(27) Morkved, T. L.; Lu, M.; Urbas, A. M.; Ehrichs, E. E.; Jaeger, H. M.; Mansky, P.; Russell, T. P. *Science* **1996**, *273*, 931−933.
(28) Thurn-Albrecht, T.; DeRouchey, J.; Russell, T. P.; Kolb, R. *Macromolecules* **2002**, *35*, 8106−8110.
(29) Boeker, A.; Knoll, A.; Elbs, H.; Abetz, V.; Mueller, A. H. E.; Krausch, G. *Macromolecules* **2002**, *35*, 1319−1325.
(30) Sakamoto, N.; Hashimoto, T. *Macromolecules* **1998**, *31*, 3292−3302.
(31) Hashimoto, T.; Sakamoto, N. *Macromolecules* **1995**, *28*, 4779−81.
(32) Sakamoto, N.; Hashimoto, T. *Macromolecules* **1998**, *31*, 8493−8502.
(33) Hohenberg, P. C.; Swift, J. B. *Phys. Rev. E* **1995**, *52*, 1828−45.
(34) Wang, W.; Hashimoto, T. *Macromolecules* **1999**, *32*, 3163−3166.
(35) Wang, W.; Hashimoto, T. *Polymer* **2000**, *41*, 4729−4735.
(36) Chastek, T. Q.; Lodge, T. P. *Macromolecules* **2004**, *37*, 4891−4899.
(37) Lin, Y.; Boeker, A.; He, J.; Sill, K.; Xiang, H.; Abetz, C.; Li, X.; Wang, J.; Emrick, T.; Long, S.; Wang, Q.; Balazs, A.; Russell, T. P. *Nature (London)* **2005**, *434*, 55−59.
(38) Chiu, J. J.; Kim, B. J.; Kramer, E. J.; Pine, D. J. *J. Am. Chem. Soc.* **2005**, *127*, 5036−5037.
(39) Bockstaller, M. R.; Lapetnikov, Y.; Margel, S.; Thomas, E. L. *J. Am. Chem. Soc.* **2003**, *125*, 5276−5277.
(40) Sohn, B. H.; Seo, B. H. *Chem. Mater.* **2001**, *13*, 1752−1757.
(41) Lodge, T. P.; Pudil, B.; Hanley, K. J. *Macromolecules* **2002**, *35*, 4707−4717.
(42) Menon, V. P.; Martin, C. R. *Anal. Chem.* **1995**, *67*, 1920−8.
(43) See Supporting Information for details.
(44) Price, C.; Chan, E. K. M.; Hudd, A. L.; Stubbersfield, R. B. *Br. Polym. J.* **1986**, *18*, 57−9.
(45) Bergues, B.; Lekki, J.; Budkowski, A.; Cyganik, P.; Lekka, M.; Bernasik, A.; Rysz, J.; Postawa, Z. *Vacuum* **2001**, *63*, 297−305.
(46) Budkowski, A.; Bernasik, A.; Cyganik, P.; Raczkowska, J.; Penc, B.; Bergues, B.; Kowalski, K.; Rysz, J.; Janik, J. *Macromolecules* **2003**, *36*, 4060−4067.
(47) da Silva, E. Z.; da Silva, A. J. R.; Fazzio, A. *Phys. Rev. Lett.* **2001**, *87*, 256102.
(48) Nicewarner-Peña, S. R.; Griffith Freeman, R.; Reiss, B. D.; He, L.; Pena, D. J.; Walton, I. D.; Cromer, R.; Keating, C. D.; Natan, M. J. *Science* **2001**, *294*, 137−141.
(49) Schultz, D. A. *Curr. Opin. Biotechnol.* **2003**, *14*, 13−22.
(50) Schoenenberger, C.; van der Zande, B. M. I.; Fokkink, L. G. J.; Henny, M.; Schmid, C.; Krueger, M.; Bachtold, A.; Huber, R.; Birk, H.; Staufer, U. *J. Phys. Chem. B* **1997**, *101*, 5497−5505.
(51) Kashchiev, D. *Nucleation: Basic Theory with Applications*; Butterworth-Heinemann: Woburn, MA, 2000.
(52) Fraaije, J. G. E. M. *J. Chem. Phys.* **1993**, *99*, 9202−12.
(53) Fraaije, J. G. E. M.; Van Vlimmeren, B. A. C.; Maurits, N. M.; Postma, M.; Evers, O. A.; Hoffmann, C.; Altevogt, P.; Goldbeck-Wood, G. *J. Chem. Phys.* **1997**, *106*, 4260−4269.
(54) Huinink, H. P.; Brokken-Zijp, J. C. M.; van Dijk, M. A.; Sevink, G. J. A. *J. Chem. Phys.* **2000**, *112*, 2452−2462.
(55) Huinink, H. P.; van Dijk, M. A.; Brokken-Zijp, J. C. M.; Sevink, G. J. A. *Macromolecules* **2001**, *34*, 5325−5330.
(56) Horvat, A.; Lyakhova, K. S.; Sevink, G. J. A.; Zvelindovsky, A. V.; Magerle, R. *J. Chem. Phys.* **2004**, *120*, 1117−1126.
(57) Sevink, G. J. A.; Zvelindovsky, A. V.; van Vlimmeren, B. A. C.; Maurits, N. M.; Fraaije, J. G. E. M. *J. Chem. Phys.* **1999**, *110*, 2250−2256.
(58) Self-consistent field (SCF) DFT methods have also been used to model the thermodynamics of nanoparticle−copolymer morphologies. See: Lee, J. Y.; Thompson, R. B.; Jasnow, D.; Balazs, A. C. *Macromolecules* **2002**, *35*, 4855−4858.
(59) Matsen, M. W.; Bates, F. S. *Macromolecules* **1996**, *29*, 1091−8.
(60) Mrozek, R. A.; Kim, B.-S.; Holmberg, V. C.; Taton, T. A. *Nano Lett.* **2003**, *3*, 1665−1669.
(61) Mrozek, R. A.; Taton, T. A. *Chem. Mater.* **2005**, *17*, 3384−3388.
(62) Suh, K. Y.; Kim, Y. S.; Lee, H. H. *J. Chem. Phys.* **1998**, *108*, 1253−1256.
(63) Knoll, A.; Horvat, A.; Lyakhova, K. S.; Krausch, G.; Sevink, G. J. A.; Zvelindovsky, A. V.; Magerle, R. *Phys. Rev. Lett.* **2002**, *89*, 035501−035504.
(64) Harrison, C.; Park, M.; Chaikin, P.; Register, R. A.; Adamson, D. H.; Yao, N. *Macromolecules* **1998**, *31*, 2185−2189.
(65) Hahm, J.; Sibener, S. J. *Langmuir* **2000**, *16*, 4766−4769.
(66) Karim, A.; Singh, N.; Sikka, M.; Bates, F. S.; Dozier, W. D.; Felcher, G. P. *J. Chem. Phys.* **1994**, *100*, 1620−9.
(67) Liu, Y.; Zhao, W.; Zheng, X.; King, A.; Singh, A.; Rafailovich, M. H.; Sokolov, J.; Dai, K. H.; Kramer, E. J.; et al. *Macromolecules* **1994**, *27*, 4000−10.
(68) van Dijk, M. A.; van den Berg, R. *Macromolecules* **1995**, *28*, 6773−8.
(69) Hochbaum, A. I.; Fan, R.; He, R.; Yang, P. *Nano Lett.* **2005**, *5*, 457−460.
(70) Mrtensson, T.; Carlberg, P.; Borgstroem, M.; Montelius, L.; Seifert, W.; Samuelson, L. *Nano Lett.* **2004**, *4*, 699−702.

MA051429J